

# RSC Advances



This is an *Accepted Manuscript*, which has been through the Royal Society of Chemistry peer review process and has been accepted for publication.

*Accepted Manuscripts* are published online shortly after acceptance, before technical editing, formatting and proof reading. Using this free service, authors can make their results available to the community, in citable form, before we publish the edited article. This *Accepted Manuscript* will be replaced by the edited, formatted and paginated article as soon as this is available.

You can find more information about *Accepted Manuscripts* in the [Information for Authors](#).

Please note that technical editing may introduce minor changes to the text and/or graphics, which may alter content. The journal's standard [Terms & Conditions](#) and the [Ethical guidelines](#) still apply. In no event shall the Royal Society of Chemistry be held responsible for any errors or omissions in this *Accepted Manuscript* or any consequences arising from the use of any information it contains.

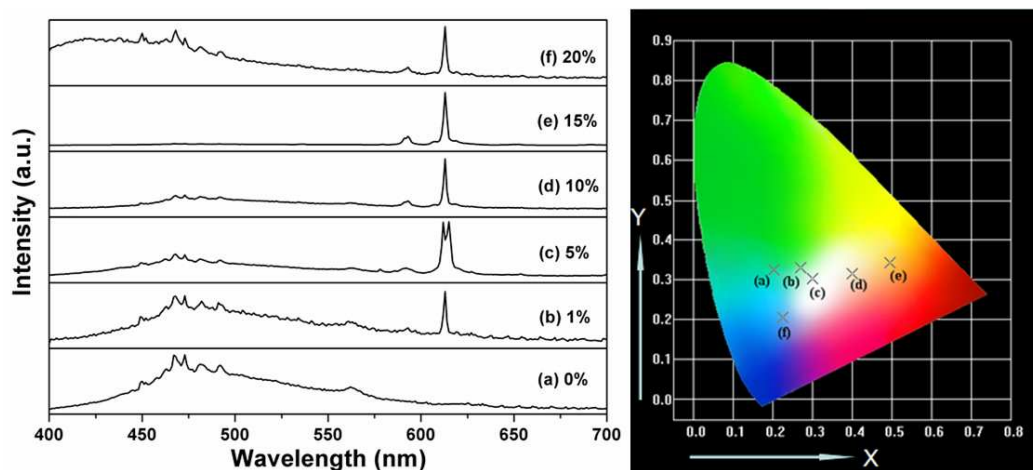
## Hydrothermal Synthesis, Characterization, and Color-Tunable Luminescence Properties of $\text{Bi}_2\text{MoO}_6:\text{Eu}^{3+}$ Phosphors

Junjun Zhang, Yali Liu, Linlin Li, Nannan Zhang, Lianchun Zou\*, Shucai Gan\*

College of Chemistry, Jilin University, Changchun 130026, PR China

\* Corresponding author: E-mail: [zoulianchun@126.com](mailto:zoulianchun@126.com) (L.C. Zou)

\* Corresponding author: E-mail: [gansc@jlu.edu.cn](mailto:gansc@jlu.edu.cn) (S.C. Gan)



$\text{Bi}_2\text{MoO}_6:\text{Eu}^{3+}$  phosphors have been successfully synthesized using a facile hydrothermal synthesis route followed by a further calcination treatment. It is clearly observed that with increasing the content of  $\text{Eu}^{3+}$ , the corresponding luminescence properties of the phosphors changed.

## Hydrothermal Synthesis, Characterization, and Color-Tunable Luminescence Properties of $\text{Bi}_2\text{MoO}_6:\text{Eu}^{3+}$ Phosphors

Junjun Zhang, Yali Liu, Linlin Li, Nannan Zhang, Lianchun Zou\*, Shucai Gan\*

College of Chemistry, Jilin University, Changchun 130026, PR China

\* Corresponding author: E-mail: [zoulianchun@126.com](mailto:zoulianchun@126.com) (L.C. Zou)

\* Corresponding author: E-mail: [gansc@jlu.edu.cn](mailto:gansc@jlu.edu.cn) (S.C. Gan)

**Abstract:** In this paper,  $\text{Bi}_2\text{MoO}_6:\text{Eu}^{3+}$  phosphors were successfully synthesized via a facile, efficient hydrothermal synthesis process followed by a further calcination treatment without using any surfactants. The samples were analyzed by XRD, UV-vis absorption spectroscopy, photoluminescence (PL) and decay curve measurements. XRD patterns reveal that all the diffraction peaks could be indexed to well-crystallized orthorhombic structure. UV-visible diffuse reflection spectra of the prepared  $\text{Bi}_2\text{MoO}_6$  and  $\text{Bi}_2\text{MoO}_6:\text{Eu}^{3+}$  indicate that they had absorption in the UV-light region. The luminescence spectra showed that  $\text{Bi}_2\text{MoO}_6:\text{Eu}^{3+}$  phosphors can be effectively excited by the UV light (328 nm), and exhibited strong red emission around 613 nm attributed to the  $\text{Eu}^{3+} {}^5\text{D}_0 \rightarrow {}^7\text{F}_2$  transition. Effects of  $\text{Eu}^{3+}$  concentration on lattice constants and PL were presented.

**Keywords:**  $\text{Bi}_2\text{MoO}_6:\text{Eu}^{3+}$ ; hydrothermal; luminescence; phosphor

## 1. Introduction

White light-emitting diodes (LEDs) are considered to be next generation solid-state lighting systems because of their excellent properties such as high luminous efficiency, energy saving, long operating time, and environmental benefit [1, 2]. There are three types of pc-LEDs; a blue-emitting LED (InGaN) coated with a yellow phosphor (YAG:Ce<sup>3+</sup>) is the most common one due to a low fabrication cost and high luminescence efficiency [3]. However, this white light has a poor heat resistance, high correlated color temperature and low color rendering index due to their low thermal quenching temperature and lack of red emitting ingredient. So, these are significant obstacles to overcome before achieving the transition to solid-state lighting [4, 5]. White LEDs using a near-ultraviolet (n-UV) LED with three primary color emissions mixed with three individual red, green, and blue-emitting phosphors have been investigated to improve the color rendering index value. This approach provides white LEDs with excellent color rendering index, but a similar drawback arises as in fluorescent lamps, owing to the strong reabsorption of the blue light by the red and green phosphors [6]. In this regard, a single-phase full-color emitting phosphor, which can be avoided by using single emitting component phosphors with higher luminous efficiency and excellent color rendering index, is considered to be potentially useful because of small color aberration, high color rendering, and low cost. Therefore the researches on single-phase full-color emitting phosphors are rapidly increasing and have become one of the hot research topics in the phosphor community [7].

Rare earth compounds have excellent properties, such as absorbing and emitting lights in all wavelengths of visible range with high color purity and stable physical and chemical properties, which attributes to the position of the 4f electrons of rare-earthions [8, 9]. And therefore they have

been widely applied in a variety of fields, such as, phosphors, LED lamps, and biological diagnose [10]. However, purer rare-earth materials are very expensive, and their ions are usually used as doped ions to dope into various host materials. Desirable host substances for rare earth ions are beneficial for practical production and application.  $\text{Bi}_2\text{MoO}_6$  is an important Aurivillius oxide, and has attracted considerable attention because of its excellent intrinsic properties and practical application, such as, gas sensors, catalytic behavior, luminescence and ion-conductive [11-14]. Because it has excellent thermal and chemical stabilities and can offer suitable sites,  $\text{Bi}_2\text{MoO}_6$  is a superb host for doping rare earth ions. To the best of our knowledge,  $\text{Bi}_2\text{MoO}_6$  have rare been studied as rare earth doped host materials.

In this research, we report the fabrication of  $\text{Bi}_2\text{MoO}_6:\text{Eu}^{3+}$  phosphors (the corresponding color tone of the phosphors shifts gradually from blue-green to white and eventually to reddish orange) via a facile, efficient hydrothermal synthesis process followed by a further calcination treatment for the first time. The effect of the doping concentration on the luminescence properties is discussed in detail. The annealed phosphors in the work have excellent photoluminescence efficiency. The obtained  $\text{Bi}_2\text{MoO}_6$ -based phosphor is coming for potential applications in the LEDs field.

## 2. Experimental section

### 2.1 Preparation of sample

$\text{Bi}(\text{NO}_3)_3 \cdot 5\text{H}_2\text{O}$  (A. R. grade),  $\text{Na}_2\text{MoO}_4 \cdot 2\text{H}_2\text{O}$  (A. R. grade), absolute ethanol and  $\text{Eu}_2\text{O}_3$  (99.99%) were purchased from Beijing Fine Chemicals Co. (China).  $\text{Eu}(\text{NO}_3)_3$  aqueous solution was obtained by dissolving  $\text{Eu}_2\text{O}_3$  in dilute  $\text{HNO}_3$  solution with heating and agitation.

All chemicals were used without further purification.

In a typical synthesis, 2 mmol (0.9702 g) of  $\text{Bi}(\text{NO}_3)_3 \cdot 5\text{H}_2\text{O}$  and 1 mmol (0.2420 g)  $\text{Na}_2\text{MoO}_4 \cdot 2\text{H}_2\text{O}$  were dissolved in 35 mL of deionized water under magnetic stirring, respectively. The two solutions were mixed together and followed by stirring for 20 min. The resulting solution was transferred into a 100 mL teflon-lined stainless steel autoclave, which was heated to  $180^\circ\text{C}$  and maintained for 12h. Subsequently, the autoclave was cooled down to room temperature naturally. The products were separated from the solution by centrifugation at 7000 rpm, washed several times with deionized water and absolute ethanol, and finally dried at  $80^\circ\text{C}$  in air for 12h. The as-prepared samples were annealed at  $500^\circ\text{C}$  for 2h.  $\text{Bi}_2\text{MoO}_6:\text{Eu}^{3+}$  samples were prepared in a similar procedure except that the corresponding  $\text{Eu}(\text{NO}_3)_3$  together with  $\text{Bi}(\text{NO}_3)_3 \cdot 5\text{H}_2\text{O}$  were added as the starting materials, as described above.

## 2.2 Characterization

The composition and phase purity of the samples were investigated by using a Rigaku D/max-II B X-ray diffractometer with graphite-monochromatic  $\text{Cu } K_\alpha$  radiation ( $\lambda = 0.15406 \text{ nm}$ ). SEM images of the products were obtained on field emission scanning electron microscope (Hitachi S-4800, Japan), employing an accelerating voltage of 5 kV. UV-vis diffuse reflectance spectra (DRS) of the samples were measured by using an Hitachi U-3010 UV-vis spectrophotometer. The PL excitation and emission spectra were recorded with a Hitachi F-7000 spectrophotometer equipped with a 150W Xe lamp as the excitation source. The PL decay curves were obtained from a Lecroy Wave Runner 6100 Digital Oscilloscope using a tunable laser (pulsewidth = 4 ns; pulse rate = 10Hz) as the excitation. All of the measurements were performed at room temperature.

## 3. Results and discussion

### 3.1. Phase identification

The composition and phase purity of the as prepared samples were first examined by XRD. The XRD patterns of obtained  $\text{Bi}_2\text{MoO}_6$  together with the Joint Committee on Powder Diffraction Standards (JCPDS) card no. 21-0102, are shown in Fig. 1a. All of the observed diffraction peaks can be indexed to those of the orthorhombic phases of  $\text{Bi}_2\text{MoO}_6$  with cell constants of  $a = 5.502 \text{ \AA}$ ,  $b = 16.213$ ,  $c = 5.483 \text{ \AA}$  [15]. No additional peaks have been found, indicating the formation of a pure phase can be easily obtained by this process. Fig. 1b shows a schematic representation of a crystal structure of  $\text{Bi}_2\text{MoO}_6$ . This crystal structure was modeled using the Run NIST/FIZ FindIt Structure and Diamond-Crystal and Molecular Structure Visualization. In  $\text{Bi}_2\text{MoO}_6$  unit cell, the crystal structure of Aurivillius type  $\text{Bi}_2\text{MoO}_6$  is composed of layers of octahedral  $[\text{MoO}_2]^{2+}$  and five-coordinated  $[\text{Bi}_2\text{O}_2]^{2+}$  linked together by layers of  $[\text{O}]^{2-}$  [16].

The XRD patterns of the samples  $\text{Bi}_2\text{MoO}_6: x\% \text{Eu}^{3+}$  ( $1 \leq x \leq 20$ ) are shown in Fig. 2a. All the diffraction peaks can be indexed to be orthorhombic phases of  $\text{Bi}_2\text{MoO}_6$ , indicating that the doped  $\text{Eu}^{3+}$  ions did not induce significant changes in the host structure. Lattice constants of the powder XRD patterns of all synthesized samples were performed in order to investigate the change of unit cell parameters as a function of  $\text{Eu}^{3+}$  concentrations. The change of lattice constants and cell volume with  $\text{Eu}^{3+}$  concentrations in the host of  $\text{Bi}_2\text{MoO}_6$  samples is shown in Fig. 2b. Since the ionic radius (coordination number (CN) = 8) of  $\text{Eu}^{3+}$  (0.106 nm) is smaller than that of  $\text{Bi}^{3+}$  (0.117 nm), the lattice constants and cell volume decrease with increasing  $\text{Eu}^{3+}$  doping concentrations. The lattice parameters  $a$ ,  $b$ , and  $c$  constantly decrease with increasing  $\text{Eu}^{3+}$  content. Similar behaviour was observed for the  $V$  ( $V = abc$ ), which gradually decreased with increasing  $\text{Eu}^{3+}$  content in the structure. This trend proves that  $\text{Eu}^{3+}$  ions can easily enter the host lattice [17].

### 3.2 Optical properties

UV-visible diffuse reflection spectrum is an important method for characterizing the optical properties of the as-prepared  $\text{Bi}_2\text{MoO}_6$  host and  $\text{Bi}_2\text{MoO}_6:\text{Eu}^{3+}$  phosphors. Fig. 3a shows the absorption spectra of sample  $\text{Bi}_2\text{MoO}_6$  (unannealed),  $\text{Bi}_2\text{MoO}_6$  (annealed),  $\text{Bi}_2\text{MoO}_6:\text{Eu}^{3+}$  (unannealed) and  $\text{Bi}_2\text{MoO}_6:\text{Eu}^{3+}$  (annealed), respectively. From the UV-vis absorption spectra we can see that the  $\text{Bi}_2\text{MoO}_6$  (unannealed),  $\text{Bi}_2\text{MoO}_6$  (annealed),  $\text{Bi}_2\text{MoO}_6:\text{Eu}^{3+}$  (unannealed) and  $\text{Bi}_2\text{MoO}_6:\text{Eu}^{3+}$  (annealed) samples show similar absorption. The steep shape of the spectra demonstrates that the absorption is induced by a band-gap transition instead of impurity levels [18]. For a crystalline semiconductor, the optical absorption near the band edge follows the equation,  $h\nu\alpha \propto (h\nu - E_{\text{gap}})^n$ , where  $\alpha$  is the absorbance,  $h$  is the Planck constant,  $\nu$  is the frequency,  $E_{\text{gap}}$  is the optical band gap, and  $n$  is a constant associated with the different types of electronic transitions. For  $n = 1/2, 2, 3/2$  and  $3$ , the transitions are the direct allowed, indirect allowed, direct forbidden, and indirect forbidden, respectively. [19]. In this work, the band gap of the  $\text{Bi}_2\text{MoO}_6$  (unannealed),  $\text{Bi}_2\text{MoO}_6$  (annealed),  $\text{Bi}_2\text{MoO}_6:\text{Eu}^{3+}$  (unannealed) and  $\text{Bi}_2\text{MoO}_6:\text{Eu}^{3+}$  (annealed) were calculated to be about 2.78, 2.70, 2.72, 2.69 eV from the onset of the absorption edge (Fig. 3b), which is consistent with previous study [20].

To examine the feasibility of the as-synthesized samples as LEDs phosphor, PL spectra of both unannealed and annealed  $\text{Bi}_2\text{MoO}_6:15\%\text{Eu}^{3+}$  powders were measured as shown in Fig. 4a. From the two spectra in Fig. 4a, one can see that the PL of the annealed powder is much more intense in comparison with that of the unannealed powder. It could be suggested that the PL intensity increased with an increase of crystallinity as shown in Fig. 4b and Fig.S1 and S2 [21].

Fig. 5a illustrates the representative of the excitation ( $\lambda_{\text{em}} = 613$  nm) and emission ( $\lambda_{\text{ex}} = 328$

nm) spectra of the  $\text{Bi}_2\text{MoO}_6:15\%\text{Eu}^{3+}$  phosphors. From Fig. 5a (left), the broad absorption band 224nm and 328nm are assigned to the host absorption (HB) and the charge-transfer band (CTB) of  $\text{O}^{2-}\rightarrow\text{Mo}^{6+}$  and  $\text{O}^{2-}\rightarrow\text{Eu}^{3+}$  groups, respectively [22, 23, 27]. The characteristic excitation spectra of the  $\text{Eu}^{3+}$  ions at 465 nm ( ${}^7\text{F}_0\rightarrow{}^5\text{D}_2$ ) can be detected. As shown in Fig.5a (right), the main emission is at 613 nm ( ${}^5\text{D}_0\rightarrow{}^7\text{F}_2$ ), originating from the electric dipole transitions of  $\text{Eu}^{3+}$ , other f-f transitions of  $\text{Eu}^{3+}$  ions, such as 593, 652 and 702 nm, relatively weak, which might be ascribed to  ${}^5\text{D}_0\rightarrow{}^7\text{F}_1$ ,  ${}^5\text{D}_0\rightarrow{}^7\text{F}_3$ , and  ${}^5\text{D}_0\rightarrow{}^7\text{F}_4$ , respectively. As we know, the  ${}^5\text{D}_0\rightarrow{}^7\text{F}_1$  transition is magnetic-dipole allowed and its intensity is almost independent of the local environment around the  $\text{Eu}^{3+}$  ions. The electric dipole transition  ${}^5\text{D}_0\rightarrow{}^7\text{F}_2$  is a hypersensitive transition due to an admixture of opposite parity  $4f^{n-1}5d$  states by an odd parity crystal-field component [24]. Therefore, the intensity ratio of the transitions  ${}^5\text{D}_0\rightarrow{}^7\text{F}_2$  to  ${}^5\text{D}_0\rightarrow{}^7\text{F}_1$ ,  $\text{R/O} = I({}^5\text{D}_0\rightarrow{}^7\text{F}_2) / I({}^5\text{D}_0\rightarrow{}^7\text{F}_1)$ , is a good measure for the symmetry of  $\text{Eu}^{3+}$  sites. The intensity of  ${}^5\text{D}_0\rightarrow{}^7\text{F}_2$  transition is much higher than that of  ${}^5\text{D}_0\rightarrow{}^7\text{F}_1$ , and the R/O values is 6.15, which is a evidence that  $\text{Eu}^{3+}$  ions mainly occupy the lattice sites without inversion symmetry [25].

Fig. 5b shows the emission spectra of  $\text{Bi}_2\text{MoO}_6:x\%\text{Eu}^{3+}$  ( $0\leq x\leq 20$ ) samples under 328nm excitation. In the undoped sample, only a broad emission of  $\text{Bi}_2\text{MoO}_6$  can be observed. With excitation at 328nm, the sample exhibit strong emission peaks at 475 nm, which is mainly attributed to the intrinsic luminescence (charge transfer transitions) within the  $\text{MoO}_6^{6-}$  complex. With the doping of  $\text{Eu}^{3+}$  ( $x = 1$ ) ions, in addition to  $\text{Bi}_2\text{MoO}_6$  host emission, we can also observe the characteristic emissions of  $\text{Eu}^{3+}$  ions. With an increase in  $\text{Eu}^{3+}$  ions concentrations ( $x = 5, 10, 15$ ), the luminescence intensity of the  $\text{MoO}_6^{6-}$  complex decreases and that of the  $\text{Eu}^{3+}$  ions photoluminescence intensity increases due to the enhancement of the energy transfer probability

from  $\text{MoO}_6^{6-}$  complex to  $\text{Eu}^{3+}$  ions. Finally, the energy is almost completely converted to the characteristic emission of  $\text{Eu}^{3+}$  ions. With the further increase the doping concentration to 20%, the luminescent intensity of  $\text{Eu}^{3+}$  ions sharply decreased due to the concentration quenching effect. This result indicates that there is an efficient energy transfer from  $\text{MoO}_6^{6-}$  to  $\text{Eu}^{3+}$  ions in  $\text{Bi}_2\text{MoO}_6:\text{Eu}^{3+}$  phosphors under UV light excitation [26].

The doping concentration of luminescent centers is an important factor influencing the phosphor performance [27]. Therefore, we investigate the emission intensities of  $\text{Bi}_2\text{MoO}_6:x\%\text{Eu}^{3+}$  ( $0 \leq x \leq 20$ ) phosphors to confirm the optimum doping concentration. The dependence of the emission intensity ( $\lambda_{\text{ex}} = 328 \text{ nm}$ ) of  $\text{Eu}^{3+}$  ions doped  $\text{Bi}_2\text{MoO}_6$  phosphors is shown in Fig. 5c. It is observed that the PL intensity of the  $\text{Eu}^{3+}$  ions first increases with increasing  $\text{Eu}^{3+}$  content and then reaches a maximum at 15 mol% for  $\text{Bi}_2\text{MoO}_6$ . After the contents of activator are over the critical value, the PL intensity decreases sharply because of the concentration quenching effect, which is mainly caused by nonradiative energy migration among the identical activator  $\text{Eu}^{3+}$  ions. The distance between the  $\text{Eu}^{3+}$  ions becomes small as the concentrations of  $\text{Eu}^{3+}$  increases; thus the probability of energy migration increases. The concentration quenching phenomena will not occur if the average distance between identical  $\text{Eu}^{3+}$  ions is so large that the energy migration is hampered; thus the critical distance ( $R_c$ ) is an important parameter which can be estimated according to the following formula [28]:

$$R_c = 2 \left( \frac{3V}{4\pi x_c N} \right)^{1/3}$$

where  $V$  is the volume of the unit cell,  $x_c$  is the critical concentration of  $\text{Eu}^{3+}$  ions, and  $N$  is the number of cations in the unit cell. For the  $\text{Bi}_2\text{MoO}_6$  host,  $V = 485.09 \text{ \AA}^3$ ,  $N = 4$  and  $x_c$  is 0.15; thus the critical distance ( $R_c$ ) is calculated to be about  $11.59 \text{ \AA}$ . The results indicate that the mechanism

of exchange interaction does not work in the energy transfer between  $\text{Eu}^{3+}$  ions in the  $\text{Bi}_2\text{MoO}_6$  hosts, because the exchange interaction is generally responsible for the energy migration between the ions with forbidden optical transitions, and the critical distance for energy transfer is restricted to about 5-8 Å. The mechanism of radiation reabsorption comes into effect only if there is a broad overlap of the fluorescent spectra of the sensitizer and activator. Thus, in view of the emission and excitation spectra of  $\text{Bi}_2\text{MoO}_6:\text{Eu}^{3+}$ , the radiation reabsorption is unlikely to occur. The energy transfer process in  $\text{Bi}_2\text{MoO}_6$  phosphors should be controlled by the electric multipole-multipole (M-M) interaction according to Dexter's theory [29].

The energy levels involved in the energy transfer process from the host to  $\text{Eu}^{3+}$  ions are depicted in Fig. 5d. Under the UV light excitation, the  $\text{MoO}_6^{6-}$  group is excited as a result of electron transfer from O 2p valence band to the Mo 4d conduction band. Subsequently, when  $\text{Eu}^{3+}$  ions were incorporated into the  $\text{Bi}_2\text{MoO}_6$  host, the energy transfer from  $\text{MoO}_6^{6-}$  to  $\text{Eu}^{3+}$ . Finally, the energy can non-radiatively relaxes from high energy level to the lower excited energy level by multi-phonon relaxation. And the multicolour emissions occur through characteristic transitions of  $\text{Eu}^{3+}$  [30].

Table 1 summarizes the CIE (Commission Internationale de L'Eclairage) chromaticity coordinates and colors and correlated color temperature (CCT) of the  $\text{Bi}_2\text{MoO}_6:x\%\text{Eu}^{3+}$  phosphors, which were calculated based on the corresponding PL spectra, and they are also represented in Fig. 6. It is clearly observed that with increasing the doping concentrations of  $\text{Eu}^{3+}$  ions, the corresponding color tone of the phosphors shifts gradually from blue-green to white and eventually to reddish orange. Hence, the white light can be realized by appropriately tuning the concentrations of the  $\text{Eu}^{3+}$  ions under the radiation of UV LED chip. More interestingly, the

sample composition of  $\text{Bi}_2\text{MoO}_6:20\%\text{Eu}^{3+}$  with CIE coordinates of (0.226, 0.206) is due to its obvious blue shift of the emission spectrum. Meanwhile, the color temperature of the samples were found to decrease gradually with increasing the doping content  $\text{Eu}^{3+}$  (< 20%) due to the variety of chromaticity coordinates.

The decay curves of  $\text{Bi}_2\text{MoO}_6:5\%\text{Eu}^{3+}$  (a) and  $\text{Bi}_2\text{MoO}_6:15\%\text{Eu}^{3+}$  (b) phosphors excited at 328 nm and monitored at 613 nm are shown in Fig. 7. The decay curves were well fitted with a second-order exponential decay mode by the following equation [31]:

$$I(t) = I_0 + A_1 \exp(-t/\tau_1) + A_2 \exp(-t/\tau_2)$$

where  $I$  and  $I_0$  are the luminescence intensities at times  $t$  and 0;  $A_1$  and  $A_2$  are constants;  $t$  is the time;  $\tau_1$  and  $\tau_2$  are the second-order exponential components of the decay time, respectively. The values of  $A_1$ ,  $\tau_1$ ,  $A_2$ , and  $\tau_2$  are obtained as shown in Fig. 7. Using these parameters, the average decay times ( $\tau_{\text{ave.}}$ ) can be determined by the formula as follows [31]:

$$\tau_{\text{ave.}} = (A_1\tau_1^2 + A_2\tau_2^2) / (A_1\tau_1 + A_2\tau_2)$$

the average lifetimes for the  $\text{Bi}_2\text{MoO}_6:5\%\text{Eu}^{3+}$  and  $\text{Bi}_2\text{MoO}_6:15\%\text{Eu}^{3+}$  are determined to be 1.748 and 0.663 ms, respectively. Z. Hou et al. reported the lifetime of  $\text{Eu}^{3+}$  ions in  $\text{Gd}_2\text{MoO}_6:\text{xEu}^{3+}$  decreases monotonically with the increasing  $\text{Eu}^{3+}$  concentrations in the studied concentrations [32]. Y. Chang et al. reported the lifetime of  $\text{Eu}^{3+}$  in  $\text{InVO}_4$  host decreases with the increasing  $\text{Eu}^{3+}$  concentration because the increasing nonradiative transition [33]. Therefore, our experimental results consistent with previous study. It is well known that in order to avoid fluorescence scintillating, the decay lifetime of phosphors used for LEDs should be short enough. It can be seen that the decay lifetime of  $\text{Bi}_2\text{MoO}_6:15\%\text{Eu}^{3+}$  (0.663 ms) is much shorter than that of  $\text{Y}_2\text{O}_3:\text{Eu}^{3+}$  (1.036ms) phosphor [34]. The decay lifetimes of  $\text{Eu}^{3+}$  in different substrates are listed in Table 2,

which basically agree with the result of our work.

#### 4. Conclusion

In summary, the phosphors of  $\text{Eu}^{3+}$  doped  $\text{Bi}_2\text{MoO}_6$  were synthesized via a facile, efficient hydrothermal synthesis process and then annealed at  $500^\circ\text{C}$  for 2h. The  $\text{Bi}_2\text{MoO}_6:15\%\text{Eu}^{3+}$  phosphor has the strongest red emission at 613 nm when excited by 328 nm wavelength. Besides, the optimum  $\text{Eu}^{3+}$  ions doping concentration is 0.15. The critical transfer distance ( $R_c$ ) based on the optimal concentration is 11.59 Å. The annealed phosphors in this work have the excellent PL efficiency. With increasing the doping concentration of  $\text{Eu}^{3+}$  ions, the corresponding color tone of the phosphors shifts gradually from blue-green to white and eventually to reddish orange. Hence, the white light can be realized by appropriately tuning the concentration of the  $\text{Eu}^{3+}$  ions in  $\text{Bi}_2\text{MoO}_6$  host under the radiation of UV LED chip.

**Electronic Supporting Information:** Fig.S1. SEM images of the as-prepared  $\text{Bi}_2\text{MoO}_6:15\%\text{Eu}^{3+}$  sample (hydrothermally treated at  $180^\circ\text{C}$  for 12h, uncalcined). Fig.S2. SEM images of the as-prepared  $\text{Bi}_2\text{MoO}_6:15\%\text{Eu}^{3+}$  sample (annealed at  $500^\circ\text{C}$  for 2h).

#### Acknowledgments

This present work was financially supported by the Mineral and Ore Resources Comprehensive Utilization of Advanced Technology Popularization and Practical Research (MORCUATPPR) funded by China Geological Survey (Grant no.12120113088300), and the Key Technology and Equipment of Efficient Utilization of Oil Shale Resources (Grant no.OSR-5). The authors thank Shasha Yi and Bingnan Wang for their cooperation and kind help in characterization.

#### References

[1] P. Waltereit, O. Brandt, A. Trampert, H. T. Grahn, J. Menniger, M. Ramsteiner, M. Reiche, K.

- H. Ploog, *Nature* 406 (2000) 865-868
- [2] C. Huang, T. Chen, *J. Phys. Chem. C* 115 (2011) 2349-2355
- [3] C. Zhao, X. Yin, Y. Wang, F. Huang, Y. Hang, *J. Lumin.* 132 (2012) 617-621
- [4] A. Katelnikovas, J. Plewa, S. Sakirzanovas, D. Dutczak, D. Enseling, F. Baur, H. Winkler, A. Kareiva and T. Jüstel, *J. Mater. Chem.* 22 (2012) 22126-22134
- [5] N. Guo, Y. Huang, H. You, M. Yang, Y. Song, K. Liu, and Y. Zheng, *Inorg. Chem.* 49 (2010) 10907-10913
- [6] T. Tam, N. Du, N. Kien, C. Thang, N. Cuong, P. Huy, N. Chien, D. Nguyen, *J. Lumin.* 147 (2014) 358-362
- [7] W. Wu and Z. Xia, *RSC Adv.* 3 (2013) 6051-6057
- [8] W. Di, X. Wang, B. Chen, S. Lu, and X. Zhao, *J. Phys. Chem. B* 109 (2005) 13154-13158
- [9] D. Chen, Y. Yu, P. Huang, H. Lin, Z. Shan, *Phys. Chem. Chem. Phys.* 12 (2010) 7775-7778
- [10] S. Kubota, Y. Suzuyama, H. Yamane, M. Shimada, *J. Alloys Compd.* 268 (1998) 66-71
- [11] Z. Zhang, W. Wang, J. Ren, J. Xu, *Appl. Catal. B: Environ.* 123-124 (2012) 89-93
- [12] R. Adhikari, B. Joshi, R. Narro-García, E. DelaRosa, S. W. Lee, *J. Lumin.* 145 (2014) 866-871
- [13] M. Zhang, C. Shao, J. Mu, X. Huang, Z. Zhang, Z. Guo, P. Zhang, and Y. Liu, *J. Mater. Chem.* 22 (2012) 577-584
- [14] T. Zhang, J. Huang, S. Zhou, L. Cao, A. Li, *Ceram. Int.* 39 (2013) 7391-7394
- [15] W. Yin, W. Wang, S. Sun, *Catal. Commun.* 11 (2010) 647-650
- [16] A. Ayame, K. Uchida, M. Iwataya, M. Miyamoto, *Appl. Catal. A: Gen.* 227 (2002) 7-17
- [17] S. Yan, Y. Chang, W. Hwang, Y. Chang, M. Yoshimura, C. Hwang, *J. Alloys Compd.* 509

(2011) 5777-5782

[18] Y. Li, J. Liu, X. Huang, *Nanoscale Res. Lett.* 3 (2008) 365-371

[19] Y. Shimodaira, H. Kato, H. Kobayashi and A. Kudo, *J. Phys. Chem. B* 110 (2006)

17790-17797

[20] C. Guo, J. Xu, S. Wang, L. Li, Y. Zhang and X. Li, *CrystEngComm*, 14 (2012) 3602-3608

[21] L. Zhang, W. Wang, Z. Chen, L. Zhou, H. Xu and W. Zhu, *J. Mater. Chem.* 17 (2007)

2526-2532

[22] L. Chen, Y. Jiang, Y. Yang, J. Huang, J. Shi and S. Chen, *J. Phys. D: Appl. Phys.* 42 (2009)

215104-215109

[23] X. Zeng, S. Im, S. Jang, Y. Kim, G. Kim, S. Kim, *J. Lumin.* 121 (2006) 1-6

[24] Y. Chang, C. Liang, S. Yan, and Y. Chang, *J. Phys. Chem. C* 114 (2010) 3645-3652

[25] G. Blasse, A. Bril, W. Nieuwpoort, *J. Phys. Chem. Solids.* 27 (1966) 1587-1592

[26] G. Li, Z. Wang, Z. Quan, X. Liu, M. Yu, R. Wang, J. Lin, *Surf. Sci.* 600 (2006) 3321-3326

[27] K. Deng, T. Gong, Y. Chen, C. Duan, and M. Yin, *Opt. Lett.* 36 (2011) 4470-4472

[28] G. Blasse, *J. Solid State Chem.* 62 (1986) 207-211

[29] H. Jing, C. Guo, G. Zhang, X. Su, Z. Yang and J. Jeong, *J. Mater. Chem.* 22 (2012)

13612-13618

[30] J. Zhang, L. Zou, S. Gan, G. Ji, *J. Phys. Chem. Solids.* 75 (2014) 878-887

[31] S. Murakami, M. Herren, D. Rau, M. Morita, *Inorg. Chim. Acta* 300-302 (2000) 1014-1021

[32] Z. Hou, H. Lian, M. Zhang, L. Wang, M. Lü, C. Zhang and J. Lin, *J. Electrochem. Soc.* 156

( 2009) J209-J214

[33] Y. Chang, Z. Shi, Y. Tsai, S. Wu, H. Chen, *Opt. Mater.* 33 (2011) 375-380

- [34] L. Li, L. Liu, W. Zi, H. Yu, S. Gan, J. Lumin. 143 (2013) 14-20
- [35] J. Liao, H. You, B. Qiu, H. Wen, R. Hong, W. You, Z. Xie, Curr. Appl. Phys. 11 (2011) 503-507
- [36] G. Jia, Y. Song, M. Yang, K. Liu, Y. Zheng, H. You, J. Cryst. Growth 311 (2009) 4213-4218
- [37] N. Niu, P. Yang, W. Wang, F. He, S. Gai, D. Wang, J. Lin, Mater. Res. Bull. 46 (2011) 333-339

**Figure Captions**

**Fig. 1.** (a) XRD pattern of  $\text{Bi}_2\text{MoO}_6$  sample synthesized by hydrothermal method (b) Crystal structure of  $\text{Bi}_2\text{MoO}_6$ .

**Fig. 2.** (a) XRD patterns of the  $\text{Bi}_2\text{MoO}_6:\text{xEu}^{3+}$  (1% - 20%) phosphors with different  $\text{Eu}^{3+}$  concentrations. (b) The  $\text{Bi}_2\text{MoO}_6:\text{xEu}^{3+}$  (1%-20%) phosphors unit cell parameters as a function of  $\text{Eu}^{3+}$  ions concentrations.

**Fig. 3.** (a) The UV-vis diffuse reflectance spectra of the  $\text{Bi}_2\text{MoO}_6$  (unannealed),  $\text{Bi}_2\text{MoO}_6$  (annealed),  $\text{Bi}_2\text{MoO}_6:\text{Eu}^{3+}$  (unannealed) and  $\text{Bi}_2\text{MoO}_6:\text{Eu}^{3+}$  (annealed) samples. (b) the plot of  $(aE)^2 \sim E$  of the corresponding samples.

**Fig. 4.** PL spectra (a) and XRD patterns (b) of both unannealed and annealed  $\text{Bi}_2\text{MoO}_6:15\%\text{Eu}^{3+}$  samples

**Fig. 5.** (a) Excitation and emission spectra of  $\text{Bi}_2\text{MoO}_6:15\%\text{Eu}^{3+}$  samples. (b) Emission spectra of  $\text{Bi}_2\text{MoO}_6:\text{x}\%\text{Eu}^{3+}$  ( $0 \leq x \leq 20$ ) phosphors with different  $\text{Eu}^{3+}$  concentrations. (c) The dependencies of the PL intensity of the samples on the contents of  $\text{Eu}^{3+}$  (x%) with an excitation of 328 nm (the intensity of  ${}^5\text{D}_0 \rightarrow {}^7\text{F}_2$ ). (d) Schematic diagram of  $\text{MoO}_4^{2-}$  and  $\text{Eu}^{3+}$  energy levels and excitation, emission, and energy transfer in  $\text{Bi}_2\text{MoO}_6:\text{Eu}^{3+}$  phosphors.

**Fig. 6.** CIE chromaticity diagram showing the emission colors for  $\text{Bi}_2\text{MoO}_6:\text{x}\%\text{Eu}^{3+}$  ( $0 \leq x \leq 20$ ) (a) 0%, (b) 1%, (c) 5%, (d) 10%, (e) 15% and (f) 20% phosphors.

**Fig. 7.** Decay curves of  $\text{Eu}^{3+}$  emission for (a)  $\text{Bi}_2\text{MoO}_6:5\%\text{Eu}^{3+}$  and (b)  $\text{Bi}_2\text{MoO}_6:15\%\text{Eu}^{3+}$  phosphors

**Table 1**

Comparison of the CIE chromaticity coordinates (x,y) and correlated color temperature (CCT) for  $\text{Bi}_2\text{MoO}_6:x\% \text{Eu}^{3+}$  (x = 0-20) phosphors.

Sample No.	Sample composition (x)	CIE coordinates (x, y)	CCT (K)
(a)	x = 0	(0.203, 0.326)	15833
(b)	x = 1	(0.271, 0.330)	9133
(c)	x = 5	(0.299, 0.303)	7716
(d)	x = 10	(0.401, 0.315)	2680
(e)	x = 15	(0.496, 0.343)	1882
(f)	x = 20	(0.226, 0.206)	844479

**Table 2**

Comparative results between the decay lifetimes of  $\text{Eu}^{3+}$  obtained in this Work and those reported in the literature in different substrates.

Substrate	Concentration (%)	Lifetime (ms)	Reference
$\text{Bi}_2\text{MoO}_6$	15	0.663	This work
$\text{Gd}_2\text{MoO}_6$	5	0.760	[32]
$\text{KLa}(\text{WO}_4)_2$	20	0.652	[34]
$\text{NaGd}(\text{WO}_4)_2$	60	0.561	[35]
$\text{YVO}_4$	5	0.625	[36]
$\text{SrMoO}_4$	5	0.510	[37]

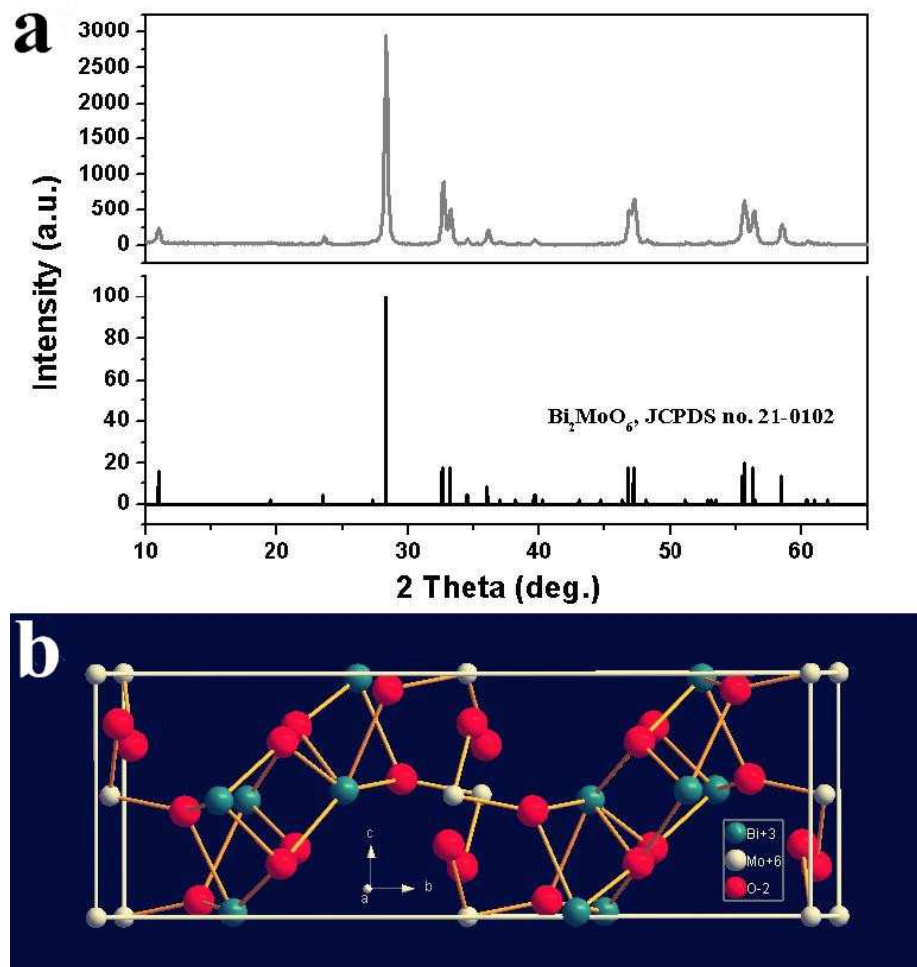


Fig. 1.

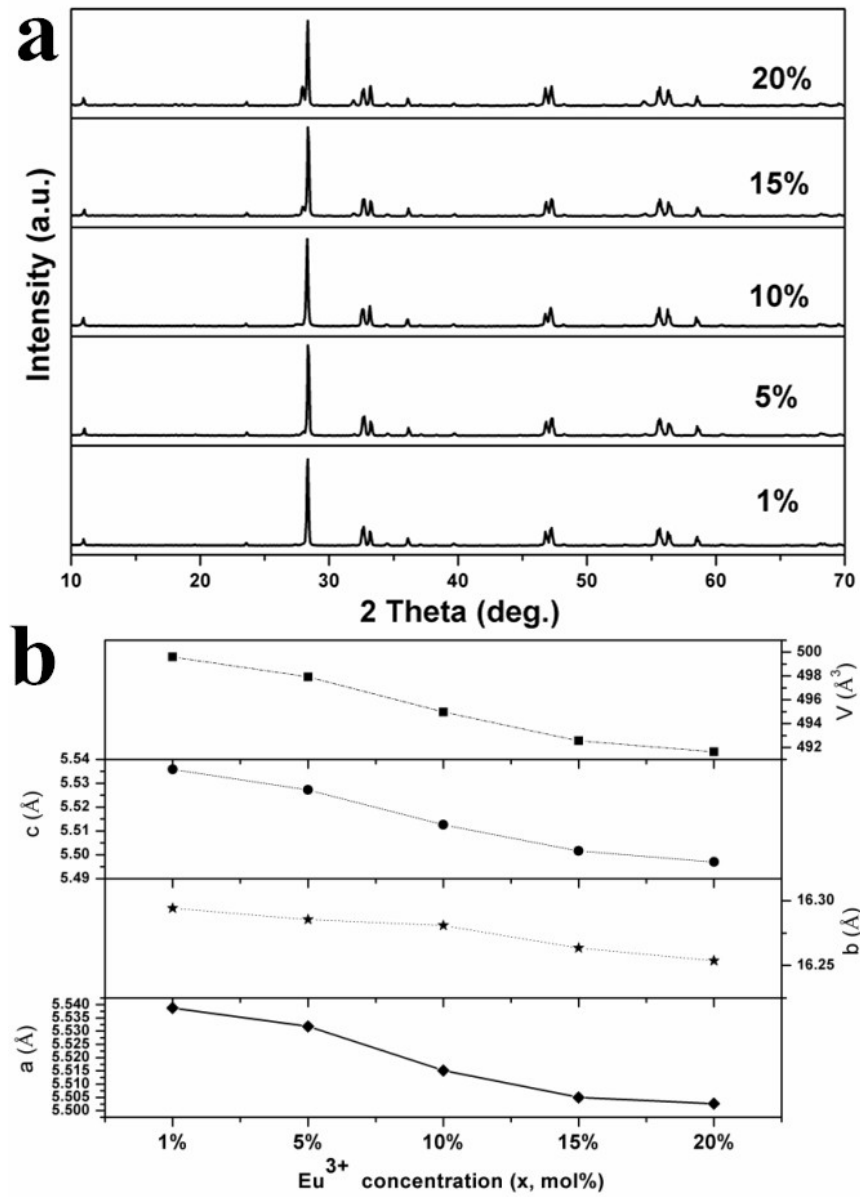


Fig. 2.

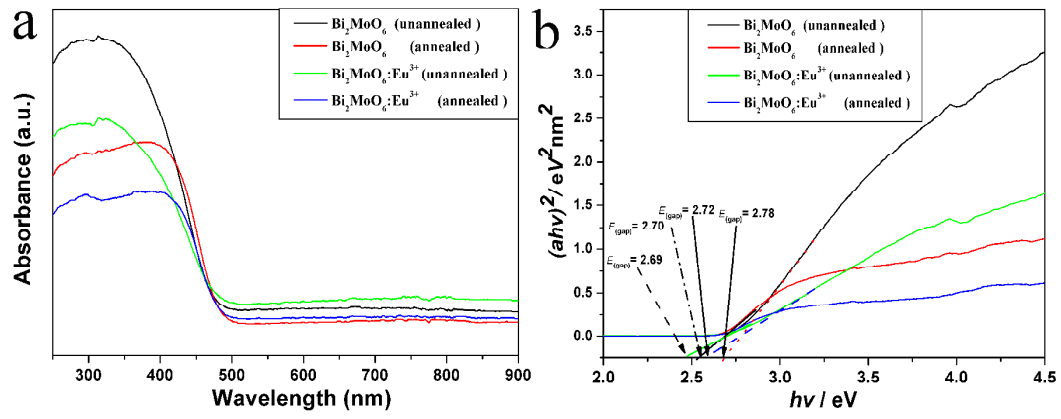


Fig. 3.

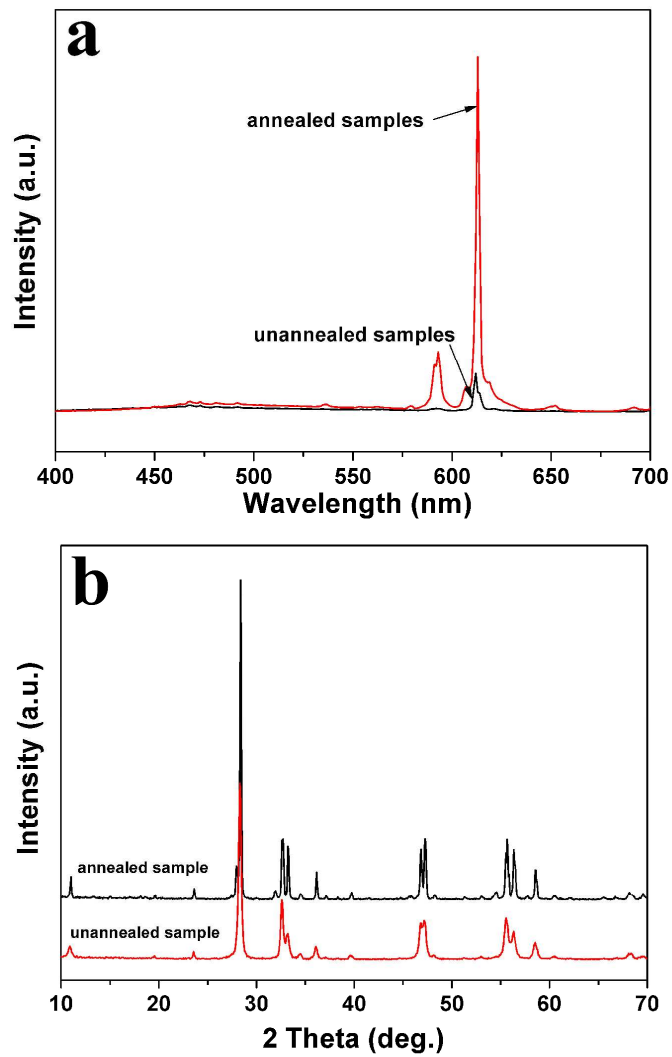


Fig. 4.

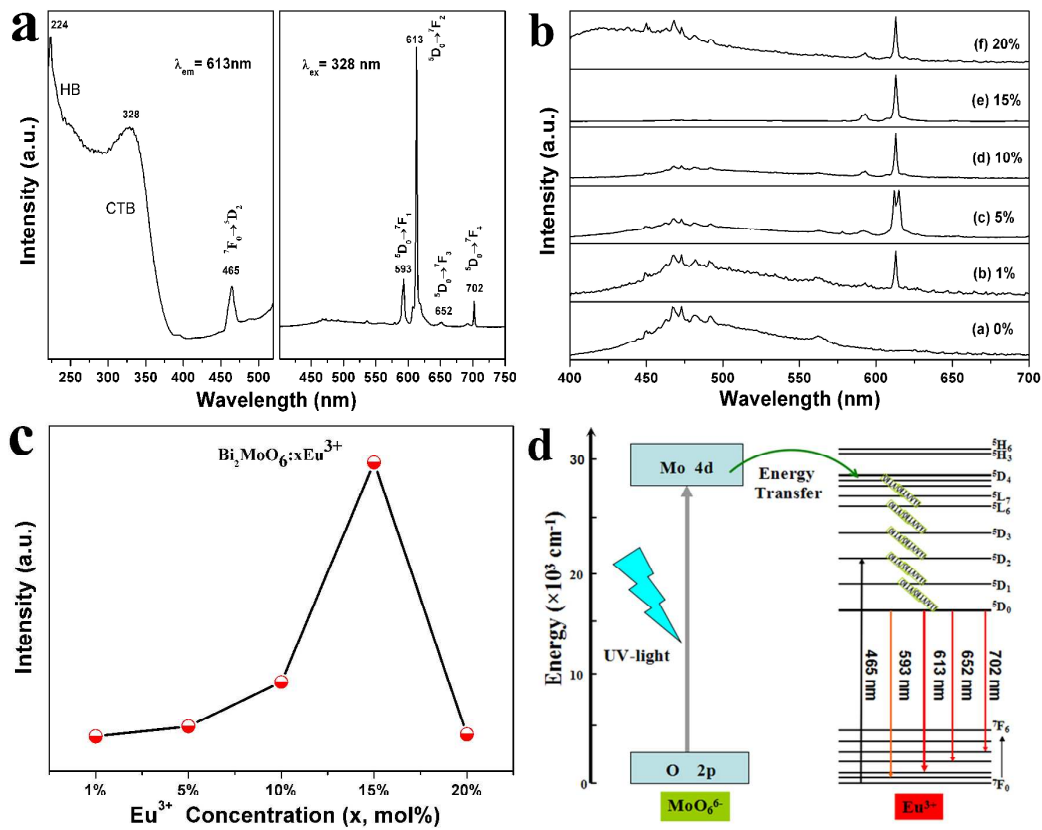


Fig. 5.

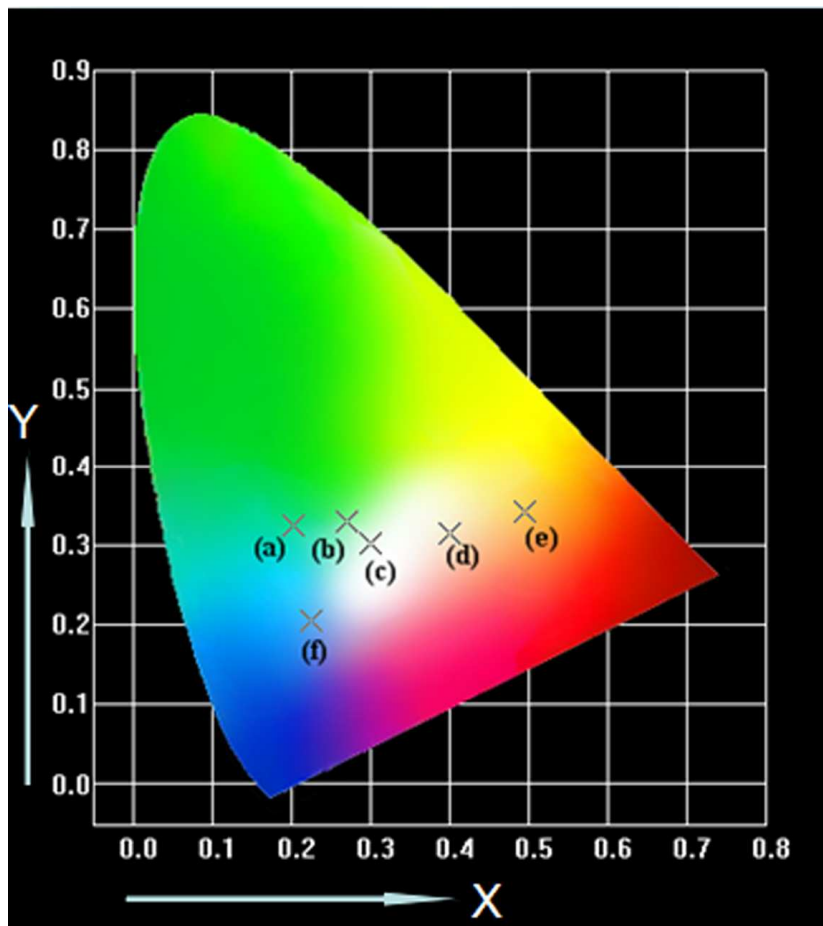


Fig. 6.

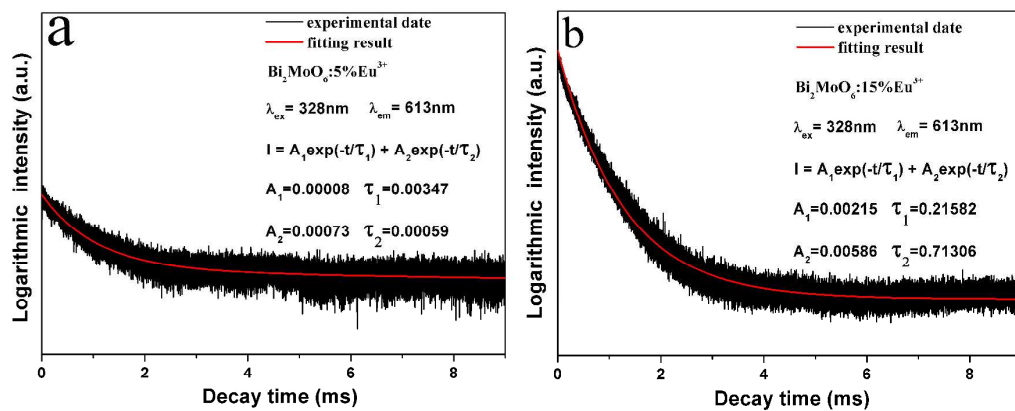


Fig. 7.